IEEE Transactions on Nuclear Science, Vol. NS-28, No. 6, December 1981

TWO-DIMENSIONAL ELECTRON BEAM CHARGING MODEL FOR POLYMER FILMS*

R.D. Reeves and K.G. Balmain
Department of Electrical Engineering
University of Toronto
Toronto, Canada M5S 1A4

Abstract

A two-dimensional model is developed to describe the charging of strips of thin polymer films above a grounded substrate exposed to a uniform mono-energetic electron beam. The study is motivated by the observed anomalous behaviour of geosynchronous satellites, which has been attributed to differential charging of the satellite surfaces exposed to magnetospheric electrons. Surface and bulk electric fields are calculated at steady state in order to identify regions of high electrical stress, with emphasis on behaviour near the material's edge. The model is used to study the effects of some of the experimental parameters, notably beam energy, beam angle of incidence, beam current density, material thickness and material width. Also examined are the consequences of a central gap in the material and a discontinuity in the material thickness.

Introduction

In the energetic-electron environment of geosynchronous satellites, exterior spacecraft dielectrics can charge electrostatically to such a degree as to cause arc discharges. Similar phenomena (first described by Gross[1] in 1957) can be caused in laboratory vacuum chambers by electron beam irradiation of insulating materials. In recent years such laboratory experiments have been widely used to approximate the satellite environment for the purpose of studying charge accumulation and the resultant discharges[2,3,4]. Theoretical modelling of the laboratory simulations has concentrated on a one-dimensional description of the charging process[3,5] which is applicable only to the centre of the specimen. The tendency of the visible discharge arc to appear brightest near the material edge suggests that such an approach may not adequately describe the necessary conditions for discharge. The NASCAP computer program can predict the complete charging response of a fully three-dimensional satellite model[6]. However in general the NASCAP cell dimensions are large compared to possible material dimensions and hence might mask edge voltage gradients by averaging of the surface voltage over the large cell area. Laboratory charging conditions have been simulated by NASCAP models by dividing the sample into small cells and requiring the voltage to fall to near-zero values at the edges[7]. It is the purpose of this paper to further quantify some aspects of the charge accumulation on long polymer strips exposed to a uniform mono-energetic electron beam that is typical of laboratory studies. Of particular interest are the resulting surface electric fields, the surface potential and the charge density near the specimen edge.

Model Description

The two-dimensional model described in this paper emphasizes those effects associated with the deflection of the incident beam by the developing charge distribution. Beam energy, beam current and material thickness are assumed to be such that space charge effects outside the sample are negligible, that the depth of the charge distribution is a small fraction of the total material thickness, and that a quasi-static description of the electric field can adequately predict the electron motion. The basic physical system modelled and the coordinate system are given in Fig.1.

The computer simulation follows the evolution of the incident current density at the material's surface as influenced by the developing charge distribution. Given the incident current density, the net charge deposition profile can be calculated as governed by the primary electron current, the backscatter current, the secondary emission current and the bulk (interior) conduction current. The charge distribution is then updated by the deposition profile and the process is repeated until an equilibrium is established. The accumulated free charge, the polarization charge in the dielectric and the effect of the ground plane are represented by an equivalent charge distribution in free space.

A Green's function formulation is used to get a closed form analytic expression for the potential and corresponding electric field of a finite-width, shallow charge layer of linearly varying density, thus creating a basic building-block for computation of the total field. In the simulation the total field is calculated at each iteration by adaptively fitting a piecewise-linear approximation to the free-space charge distribution subject to a root-mean-square error tolerance of 1.5% of the distribution average and then summing each segment's contribution. Typical fits at equilibrium require approximately 15 segments to satisfy the above criteria. Using this set of fields a third-order Runge-Kutta method with an adaptive time increment subject to a local error constraint on the incident electron position and velocity of 0.2 μm and 2.0×10^5 m/sec. respectively was used to calculate the selected electron trajectories used to scan the surface. The incident current density at the material surface is deduced from the relative spreading between adjacent trajectories.

The accumulation of charge is described by the following difference equation: $\Delta\rho = \Delta t(J_i - J_{bs} - J_{se} - J_c)$ where $\Delta\rho$ is the net change in the local surface charge density, Δt is the time increment and J represents the current density components. We shall use the convention that a current density refers to a transfer of negative charge normal to the surface of the material. A summary of the empirical relationships used to describe the charging process is found in Table 1. The energy of impact KE and the angle of impact θ are obtained directly from the trajectory calculations.

Results and Discussion

The charging of a dielectric can be classified as either conduction-limited or emission-limited, at low or high incident-beam current densities respectively. This behaviour is readily apparent in the equilibrium surface potential as illustrated in Fig.2 for normally incident electrons. A steady state is achieved when the net current to the surface is zero, suggesting that $J_i(1 - SE - BS) = J_c$ where SE is the secondary emission coefficient and BS is the backscatter coefficient. If $J_i/J_c \approx 1$ then $V = (1 - SE - BS)\, J_i d/g$ where $KE = BE$. If $J_i/J_c \gg 1$ then $V = (BE - KE_2)/e$ where KE_2 is the second unity emission energy at which $SE + BS = 1$. The critical current density separating the two regimes can be calcu-

*Work supported by the U.S.Air Force Weapons Laboratory and by NASA through Grant NSG-7647, and by the Natural Sciences and Engineering Research Council of Canada, through Operating Grant A-4140.

0018-9499/81/1200-4547$00.75©1981 IEEE

lated by equating the two asymptotic expressions. Substituting typical charging conditions (beam energy 20 keV, sample thickness 50 μm, conductivity 3.3×10^{-18} $(\Omega cm)^{-1}$), the critical current density for Teflon is found to be 0.03 nA/cm^2. The transition from conduction-limited to emission-limited charging occurs over a single decade range in current densities for Teflon, for which the two-dimensional simulations have been confined to emission-limited mechanisms representative of typical charging situations. For Kapton, the field-dependent conductivity must be included even for relatively high current densities. Using the same charging conditions with the field-dependent conductivity suggested in Table 1, the surface potential is found to vary approximately as $J_i^{0.22}$ in the interval 0.1 - 100.0 nA/cm^2. This appears to be consistent with Kapton discharge measurements made by Balmain and Hirt[2] indicating that the released charge varies as $J_i^{0.23}$ over the same range of current density.

In two dimensions, the second unity emission energy KE_2 is a function of the angle of incidence θ. A total emission coefficient described by Robinson and Budd[8] which varies as 1/cos θ and $KE^{-0.58}$ should tend to produce a slightly flatter central surface potential than those results described later in this paper.

Results and Discussion: Teflon

The equilibrium net charge profiles, for 100 μm thick Teflon simulations, irradiated with beam energies ranging from 5 to 25 keV are given in Fig.3 (sample half-width 0.75 cm, sample thickness 100 μm, data collected at 160 equally spaced points across the sample). The charge distribution and the corresponding surface potential (Fig.4) are approximately proportional to (BE-2.1) keV across the entire sample. Also shown in Fig.4 are potential measurements made by Robinson[9], taken across the diameter of a circular sample (experiment: Teflon, 127 μm thick, circular aperture 2.5 cm diam. cut in 1.3 mm thick aluminium plate), and by Stevens et al[14] taken across the centre of long strips of silvered Teflon (experiment; silver-backed Teflon strips 130 μm thick above a flat ground plane, sample areas tested 10 × 20 cm^2 and 15 × 20 cm^2). All three sets of data show good agreement with the computed results. The bulk electric field can be estimated from the surface potential and the material thickness. The surface electric fields are presented in Figs.5 and 6. The steps in the surface field profiles are computational artifacts resulting from the discontinuities in the slope of the piecewise linear approximation for the charge profile used in their calculation. The positioning of the linear segments is randomized between successive iterations thus minimizing the cumulative effect of the field artifacts on the developing charge and surface potential distributions. The field profiles at heights greater than 2d (i.e. 200 μm) above the charge plane show no such artifacts.

The calculation of the surface tangential field is complicated by a logarithmic singularity at the material edge for a uniform surface charge distribution. The field a distance Δy above the edge is proportional to $\ell n(2d/\Delta y)$ where d is the material thickness. By integrating this expression, the tangential field in the centre of a uniform volume charge distribution of depth S is found to be proportional to $\ell n(10.9d/S)$. Since the details of the internal charge migration are not well known we have evaluated all surface fields at a fixed reference $d/\Delta y = 100$. Rescaling the edge results for an alternative charge distribution can be accomplished with the above formulas.

The equilibrium surface potential for half-widths W ranging from 1.5 cm to 1.5/8 cm is presented in Fig.7 (beam energy 20 keV, sample thickness 100 μm). Note that the surface potential over most of the sample can be described by a single scale length x/W; the data presented in Fig.4 having been measured on samples ranging from 5 - 300 cm^2 in area supports this result. The edge surface fields were found to vary as $W^{-0.7}$ and $W^{-0.3}$ for the normal and tangential components respectively. In the centre both surface components varied as $W^{-1.0}$.

The equilibrium surface charge and bulk fields were found to be inversely proportional to the material thickness over the entire material surface. The surface potential and surface fields were found to be independent of the material thickness except for the tangential field at the edge which varied as $d^{-0.61}$.

The equilibrium net charge profiles for specimens exposed to beams ranging in angle of incidence from 0° to 45° are given in Fig.8 (beam energy 20 keV, sample thickness 100 μm, sample half-width 0.75 cm.). The corresponding surface potentials and surface fields are given in Figs.9, 10 and 11. The maxima for both the potential and charge density were found to shift toward the edge closest to the electron source. The maximum surface fields, also found at the source edge, were found to vary as $10^{0.0104\theta}$ with θ in degrees. At the far edge the fields were found to decrease with increasing beam angle.

Simulations used to investigate the effect of a central gap in the irradiated material included gap widths of 0.0283 cm and 0.066 cm representing 1.9% and 4.4% of the full sample width (beam energy 20 keV, sample thickness 100 μm and sample half width 0.75 cm). The equilibrium charge density in Fig.12 shows a sharp increase in the distribution near the gap edges. The resulting surface fields are given in Figs.13 and 14. A set of representative trajectories in Fig.15 indicates the degree of beam steering that occurs as the sample approaches steady state.

The equilibrium net charge profiles in Fig.16 were obtained for a composite material consisting of two adjacent uniform sections with sample thicknesses of 50 and 100 μm (beam energy 15 keV, sample half width 0.75 cm). The distribution of charge is such that the dipole moment $\rho(x)d$ across the sample is similar to that found for a uniform sample. The resulting surface potential displays a sharp depression of 8.0 kV at the transition in thickness and the associated surface fields are given in Figs.17 and 18.

Results and Discussion: Kapton

The charging characteristics of Kapton are illustrated at beam current densities of 100 nA/cm^2 and 1 nA/cm^2. The higher current density simulation is representative of the emission-limited mechanism noted in Teflon. The lower current density simulation is representative of conduction-limited charging. The charging conditions were: beam energy 20 keV, material thickness 50 μm, material half-width 0.75 cm.

The equilibrium net charge density profiles are given in Fig.19. The high-current simulation indicates a broad maximum in the centre of the sample whereas the low-current case produces a uniform charge distribution. If the conduction current were neglected both curves would be equal and would reach a maximum charge density at the centre of 1.2 μC/cm^2. The steady-state surface potential is presented in Fig.20. The peak tangential field of approximately 2×10^6 V/cm is comparable for both cases although for the uniform charge distribution it is less than 10^4 V/cm over 98% of the surface compared to 79% for the higher current density.

Tangential currents confined to the radiation-induced conductivity layer at the material's surface were investigated for Kapton. The preliminary results indicate no significant effects.

Conclusions

A two-dimensional model has been presented to describe the deposition of charge on long dielectric strips by a uniform monoenergetic electron beam used to simulate spacecraft charging conditions. Numerical results

for Teflon and Kapton indicate that both tangential and normal surface field peaks occur near the metal-dielectric edge. The tangential component was found to be dominant with a field strength of the order 10^6 V/cm. The edge fields were found to increase with increasing beam angle and energy and decrease with increasing material width and thickness. The degree of beam steering near steady state, for emission-limited charging conditions, suggests that multi-dimensional analyses are crucial for a complete understanding of the charging process. Under conduction-limited charging conditions, the one-dimensional models appear to predict accurately the final charge distribution.

References

1. Gross, B., "Irradiation Effects in Borosilicate Glass", Phys. Rev., Vol.107, No.2, July 1957, pp. 368-373.
2. Balmain, K.G. and Hirt, W. "Dielectric Surface Discharges: Dependence on Incident Electron Flux", IEEE Trans. Nucl. Sci., Vol.NS-27, No.6, Dec.1980, pp.1770-1775.
3. Purvis, C.K., Stevens N.J. and Oglebay J.C. "Charging Characteristics of Materials: Comparison of Experimental Results with Simple Analytic Models", Proceedings of the Spacecraft Charging Technology Conference, C.P. Pike and R.R. Lovell eds., NASA TMX-73537, 1977, pp.459-486.
4. Yadlowsky, E.J., Hazelton, R.C. and Churchill, R.J., "Characteristics of Edge Breakdown on Teflon Samples", IEEE Trans. Nucl. Sci., Vol.NS-27, No.6, Dec. 1980, pp.1765-1769.
5. Beers, B.L., Hwang, H., Lin, D.L. and Pine, V.W., "Electron Transport Model of Dielectric Charging", Spacecraft Charging Technology - 1978, NASA CP-2071, 1979, pp.209-238.
6. Katz, I., Parks, D.E., Mandell, M.J., Harvey, J.M., Brownell, D.H., Wang, S.S. and Rotenberg, M., "A Three Dimensional Dynamic Study of Electrostatic Charging in Materials", NASA CR 135 256, 1977.
7. Stevens, N.J., "Computer and Laboratory Simulation of Interactions Between Spacecraft Surfaces and Charged-Particle Environments", NASA TM 79219 July 1979.
8. Robinson, J.W. and Budd, P.A.,"Oblique-incidence Secondary Emission", paper presented at the USAF/NASA Spacecraft Charging Technology Conference, Colorado Springs, 1980.
9. Robinson, J.W., "Charge Distributions Near Metal-Dielectric Interfaces Before and After Dielectric Surface Flashover", Proceedings of the Spacecraft Charging Technology Conference, C.P. Pike and R.R. Lovell eds., NASA TMX-73537, 1977, pp.503-516.
10. Burke, E.A., "Secondary Emission from Polymers", IEEE Trans. Nucl. Sci., Vol.NS-27, No.6, Dec.1980, pp.1760-1764.
11. Wall, J.A., Burke, E.A. and Frederickson, A.R.,"Results of a Literature Search on Dielectric Properties and Electron Interaction Phenomena Related to Spacecraft Charging", Proceedings of the Spacecraft Charging Technology Conference, C.P. Pike and R.R. Lovell eds., NASA TMX-73537, 1977, pp. 569-592.
12. Adamec, V. and Calderwood, J.H., "Electrical Conduction in Dielectrics at High Fields", Journal of Phys. D: Appl. Phys., Vol.8, 1975, pp.551-560.
13. Adamo, R.C. and Nanevicz, J.E., "Conductivity Effects in High-Voltage Spacecraft Insulating Materials", Proceedings of the Spacecraft Charging Technology Conference, C.P. Pike and R.R. Lovell eds., NASA TMX-73537, 1977, pp.669-686.
14. Stevens, N.J., Purvis, C.K. and Staskus, J.V. "Insulator Edge Voltage Gradient Effects in Spacecraft Charging Phenomena", IEEE Trans. Nucl. Sci., Vol.NS-25, No.6, Dec. 1978, pp.1304-1312.

Table 1

Description	Functional Form(Units)
Beam curr. dens., J_b	(A/cm^2)
Incident curr.dens., J_i	
Secondary emission curr.dens., J_{se}	J_i SE
Backscatter curr. dens., J_{bs}	J_i BS
Conduction curr. dens., J_c	g E
Second. emiss. coeff.[10], SE	$K\,KE^{-0.725}\exp(2(1-\cos\theta))$
	K = 1.55, Teflon
	K = 0.68, Kapton
Backscatter coeff.[11], BS	$(0.1\,KE^{-0.2})\cos\theta$
	Teflon and Kapton
Electric field, E	(V/cm)
Conductivity[5,12,13], g, Teflon	$\approx 3.3\times10^{-18}(\Omega cm)^{-1}$
Kapton	$\approx g_o(2+\cosh(4.68\times10^{-3}E))/3$
	$g_o \approx 5\times10^{-18}(\Omega cm)^{-1}$
Beam energy, BE	(keV)
Electron kinetic energy, KE	(kev)
Angle to surface normal, θ	
Surface potential magnitude, V	(kV)
Electron charge magnitude, e	(C)
Unity emiss. energy, KE_2	$SE(KE_2,\theta)+BS(KE_2,\theta)=1$

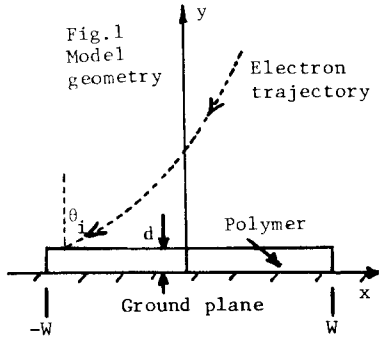

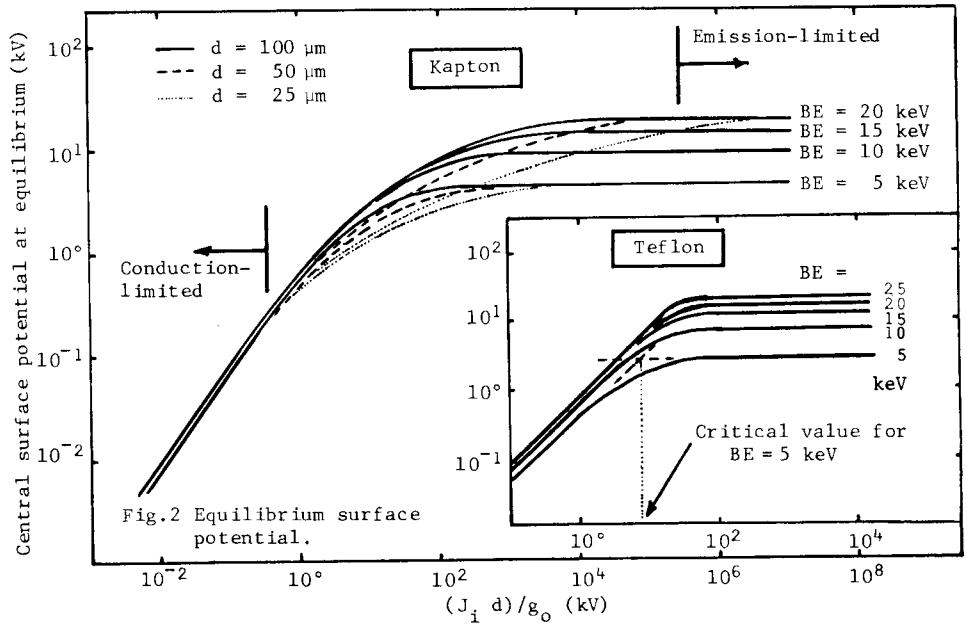

Fig.2 Equilibrium surface potential.

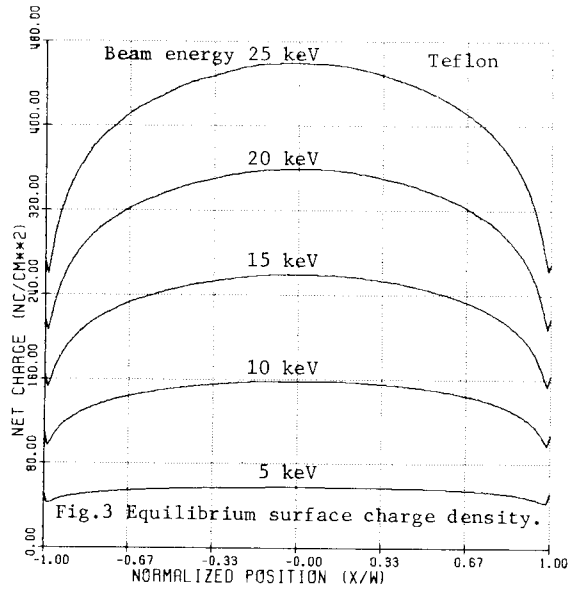

Fig.3 Equilibrium surface charge density.

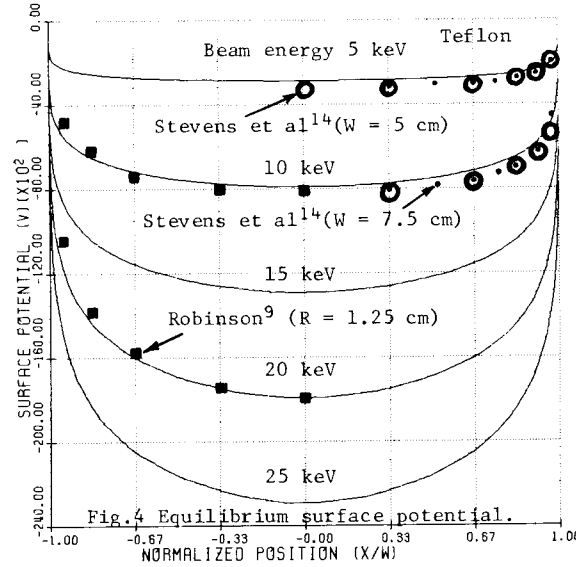

Fig.4 Equilibrium surface potential.

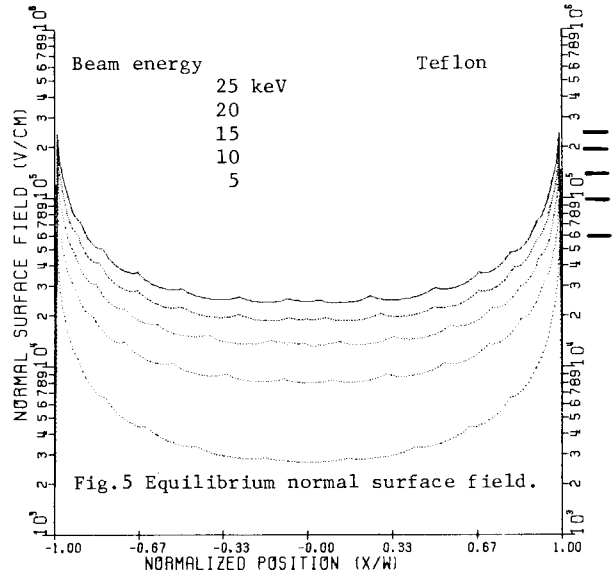

Fig.5 Equilibrium normal surface field.

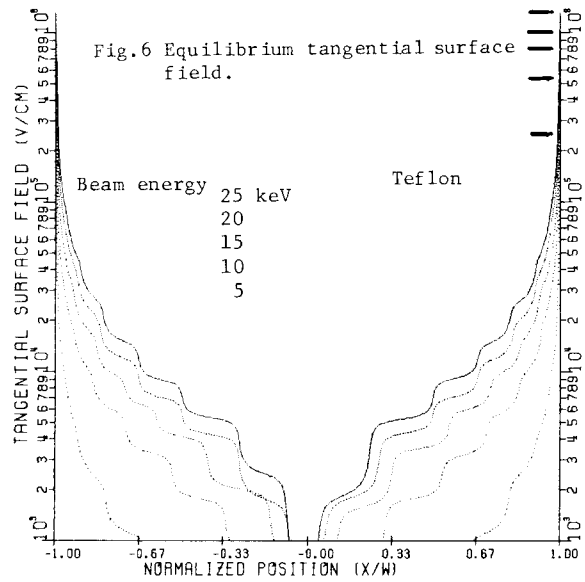

Fig.6 Equilibrium tangential surface field.

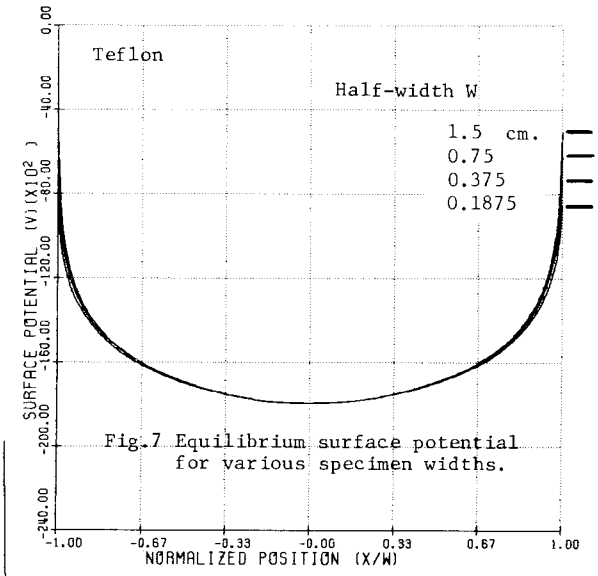

Fig.7 Equilibrium surface potential for various specimen widths.

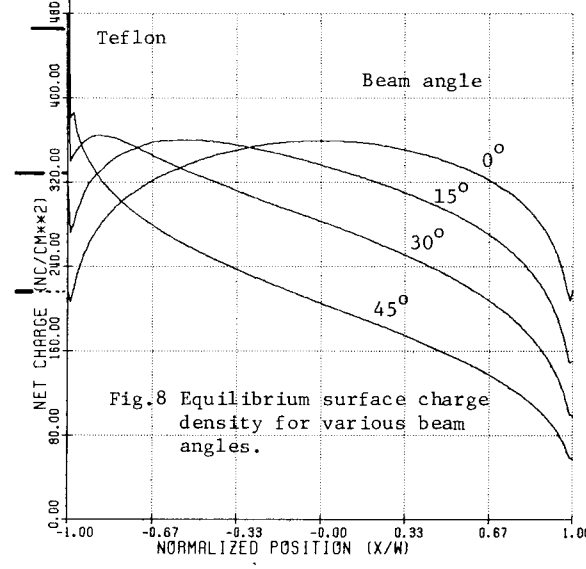

Fig.8 Equilibrium surface charge density for various beam angles.

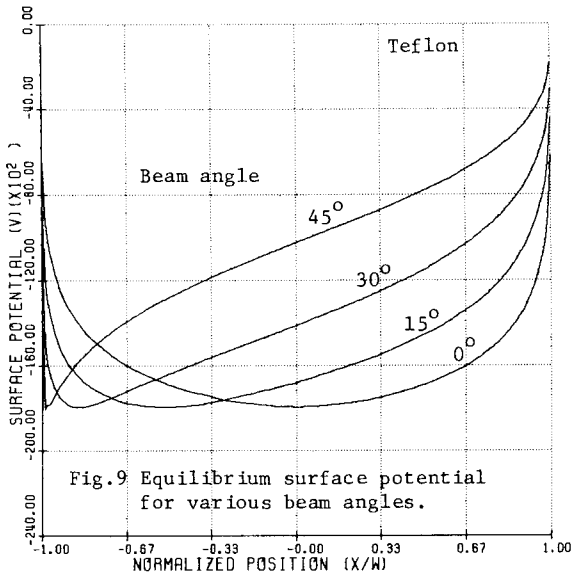

Fig.9 Equilibrium surface potential for various beam angles.

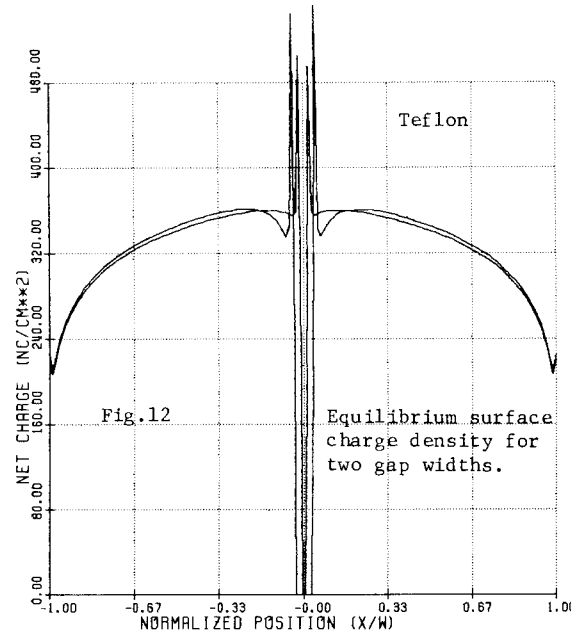

Fig.12 Equilibrium surface charge density for two gap widths.

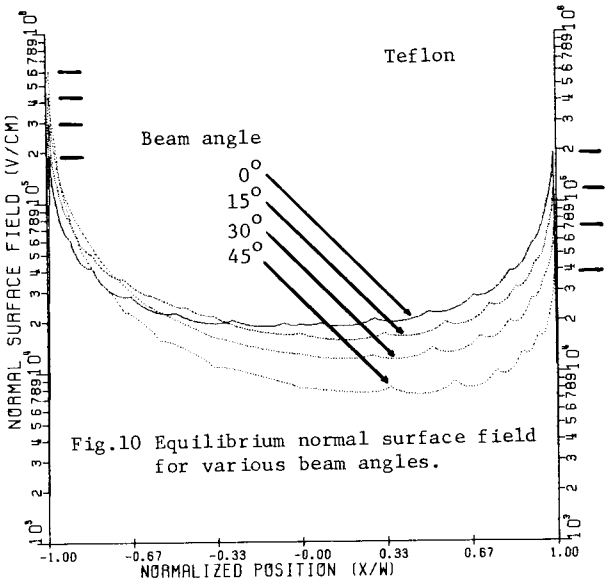

Fig.10 Equilibrium normal surface field for various beam angles.

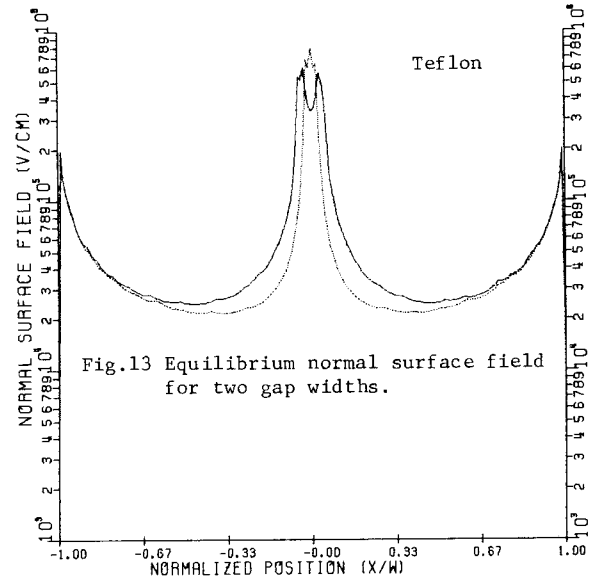

Fig.13 Equilibrium normal surface field for two gap widths.

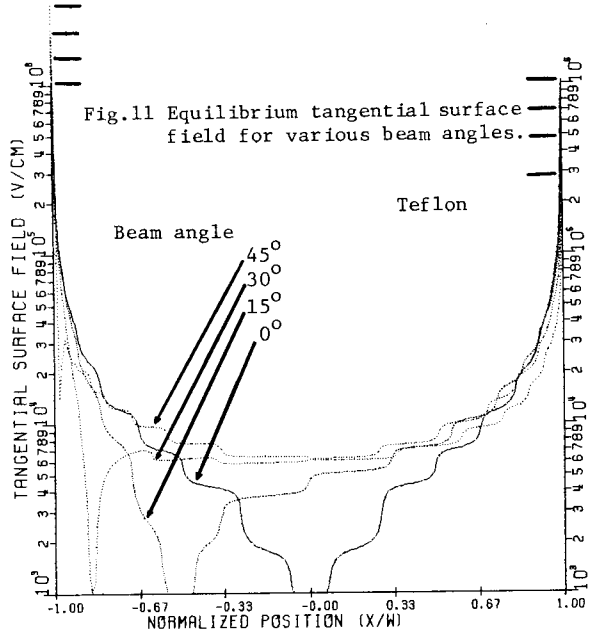

Fig.11 Equilibrium tangential surface field for various beam angles.

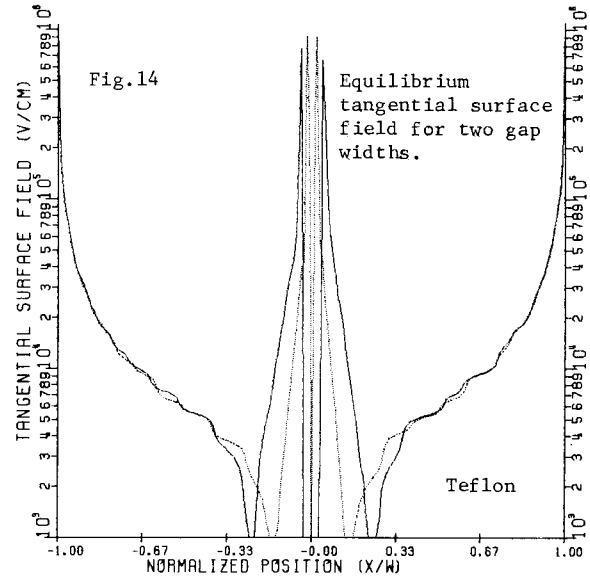

Fig.14 Equilibrium tangential surface field for two gap widths.

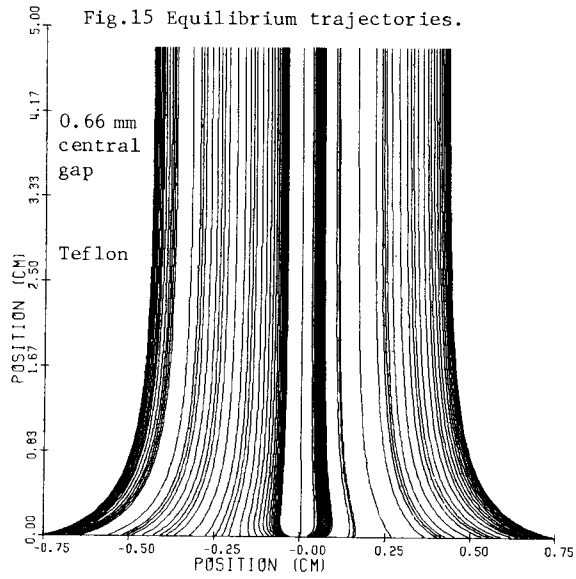

Fig.15 Equilibrium trajectories.

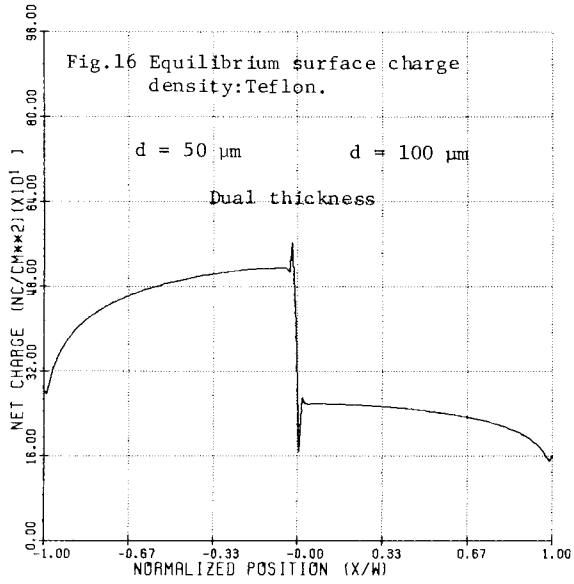

Fig.16 Equilibrium surface charge density:Teflon.

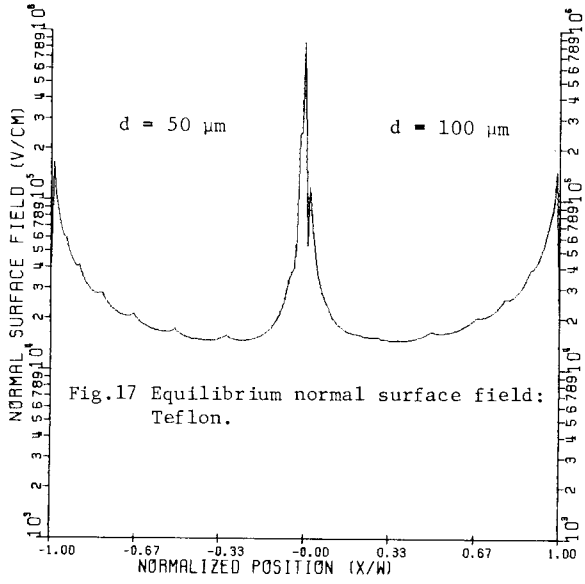

Fig.17 Equilibrium normal surface field: Teflon.

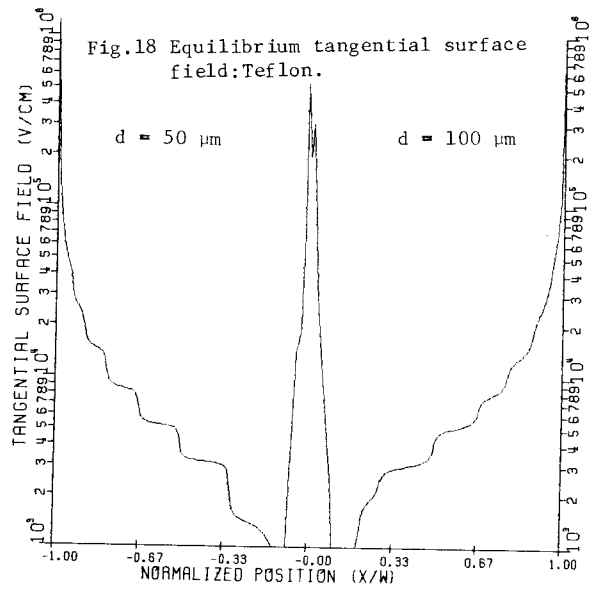

Fig.18 Equilibrium tangential surface field:Teflon.

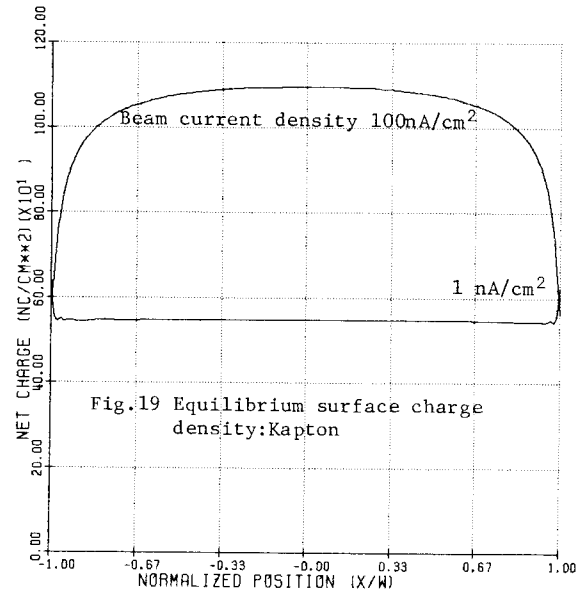

Fig.19 Equilibrium surface charge density:Kapton

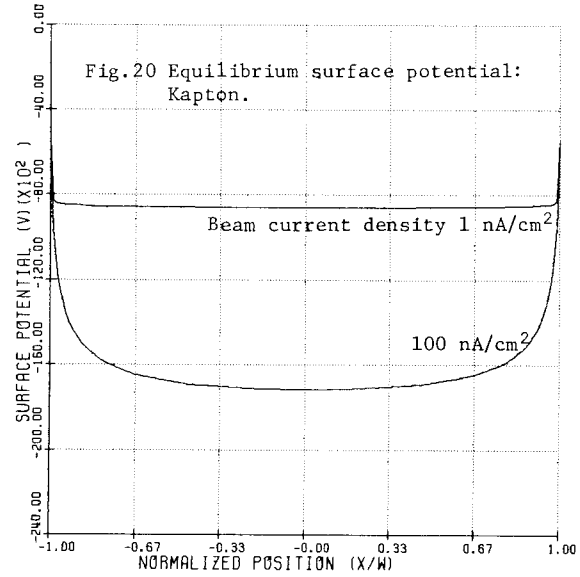

Fig.20 Equilibrium surface potential: Kapton.